2,2'-Dipyridylamine as Heterogeneous Organic Molecular Electrocatalyst for Two-Electron Oxygen Reduction Reaction in Acid Media

*Xi Yin, Ling Lin, Ulises Martinez, and Piotr Zelenay**

Materials Physics and Applications Division, Los Alamos National Laboratory,

Los Alamos, NM 87545, USA

ABSTRACT Continuous production of hydrogen peroxide (H_2O_2) through the two-electron oxygen reduction reaction (2e-ORR) in distributed electrochemical cells offers important advantages for point-of-use water treatment and pulp bleaching over the complex industrial anthraquinone process. A low-cost, heterogeneous 2e-ORR electrocatalyst with high activity and selectivity is key to meeting the future needs for distributed production of H_2O_2 with large capacity. Herein, we demonstrate high activity and selectivity of a new heterogeneous organic molecular electrocatalyst, 2,2'-dipyridylamine, with an H_2O_2 yield of *ca.* 80%, and an onset potential of *ca.* 0.60 V *vs.* RHE in acidic aqueous electrolyte. We show that this acid-compatible, inexpensive, small organic molecule can catalyze 2e-ORR as efficiently as the state-of-the-art catalysts based on mercury-precious metal alloys. We propose different mechanisms of dioxygen electroreduction based on density functional theory calculations, which correlate activity with calculated standard reduction potential of reaction intermediates.

KEYWORDS Heterogeneous electrocatalysis; two-electron oxygen reduction reaction; 2e-ORR; hydrogen peroxide; H_2O_2; 2,2'-dipyridylamine; organic molecular electrocatalyst; organic catalyst.

TOG Graphic

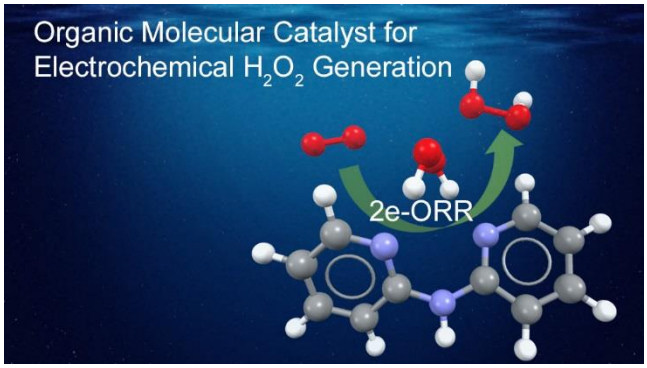
Organic Molecular Catalyst for
Electrochemical H_2O_2 Generation
2e-ORR

Introduction

Hydrogen peroxide (H_2O_2) is an important chemical with versatile applications in water treatment, environmental remediation, paper/pulp industry, production of bleach, and medical disinfection.[1,2] Industrial production of H_2O_2 relies on the anthraquinone process, which has many drawbacks, such as complexity, high initial capital cost, and added transportation and distribution cost.[1,2] By comparison, the electrochemical production of H_2O_2 in fuel cell and electrolyzer setups has attracted much attention thanks to its safety, energy efficiency and capacity to be conducted in distributed systems.[1,3-8] Such systems require an efficient and highly selective heterogeneous catalyst for two-electron oxygen reduction reaction (2e-ORR) to generate H_2O_2. Catalysts explored for electrochemical production of H_2O_2 include carbons,[4,6,9-11] heteroatom-doped carbon materials,[12-14] carbon-coated precious metals,[15] atomically dispersed platinum,[16] and metal nanoparticles based on precious metal-mercury alloys.[17,18] Because of a better H_2O_2 stability in acids and maturity of the proton exchange membrane (PEM) devices, 2e-ORR catalysts capable of operating in acidic environments are generally preferred. Low-cost carbon and heteroatom-doped carbon materials have shown good activity for 2e-ORR in alkaline solutions but significantly lower activity and selectivity in acidic electrolytes[9,10,13] Mercury-precious metal alloys have demonstrated high selectivity and activity in acidic electrolytes,[17,18] but their cost and potential risk of mercury release make them less appealing for practical applications.

Besides the materials mentioned above, some organic molecules have also shown catalytic activity for the 2e-ORR. They include quinones,[19-22] viologens,[23-28] pyrazine derivatives,[29-32] and porphyrin-type macrocycles.[33-39] While these organic molecular catalysts are based on well-defined chemical motifs that allow for structure-activity correlations and activity fine-tuning, they are not fully viable for H_2O_2 production. For instance, viologens and porphyrins are

homogeneous catalysts that require a solution phase, less attractive than heterogeneous systems. Quinones and viologens have good 2-e ORR activity in alkaline electrolytes but perform poorly in acidic electrolytes. For pyrazine derivatives, high overpotential is needed to catalyze 2e-ORR in acidic environments. Furthermore, only a few organic structural motifs have been explored for their catalytic activity, leaving the vast organic chemical space unexplored. Well-defined organic molecular electrocatalysts with low cost, high activity and selectivity for 2e-ORR in acidic electrolyte are needed to enable energy-efficient and cost-effective electrochemical production of H_2O_2.

Herein, we demonstrate 2,2'-dipyridylamine (dpa) adsorbed on glassy carbon support (**Scheme 1**), as an efficient heterogeneous and inexpensive organic molecular electrocatalyst for the 2-e ORR to generate hydrogen peroxide in acidic aqueous electrolytes.

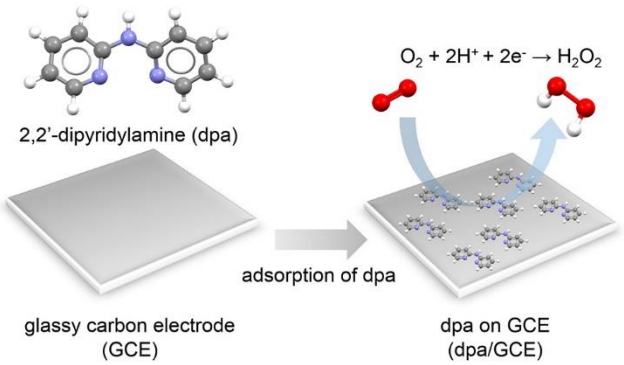

Scheme 1. Heterogeneous organic molecular catalyst based on 2,2'-dipyridylamine adsorbed on glassy carbon substrate for two-electron reduction of dioxygen.

Results and Discussion

We evaluated the 2e-ORR activity of dpa adsorbed on glassy carbon electrode (GCE) in a standard three-electrode electrochemical cell, using graphite rod as a the counter electrode and a hydrogen reference electrode (HydroFlex®, Gaskatel GmbH). **Figure 1** shows a rotating ring-disk electrode (RRDE) polarization curve of dpa on glassy carbon disk electrode (dpa/GCE) in O_2-saturated 0.5 M H_2SO_4 solution at 25 °C, using a 20-mV potential steps from 0.8 V to 0 V and 20-second hold time per step. The onset potential of the 2e-ORR was *ca.* 0.60 V *vs*. RHE, close to the thermodynamic equilibrium potential of 0.70 V. The current density increased to *ca.* 1.5 mA/cm^2 at 0 V, exceeding the theoretical limiting current density for 100% 2e-ORR by 6%. Data in Figure 1b reveal a *ca*. 80% H_2O_2 yield at the dpa/GCE catalyst and current efficiency (CE) of *ca.* 67% in the potential range of 0 to 0.4 V *vs.* RHE, based on the ring current. Here, we define the H_2O_2 yield as the molar fraction of H_2O_2 in the product of H_2O_2/H_2O mixture, and the current efficiency as a ratio of electrons consumed in the 2e-ORR to the total number of electrons transferred.

In order to make sure that that peroxide generation was happening only at the molecular catalyst, we took special care to minimize the presence of trace metal impurities during the experiments. The trace amounts of potentially ORR-active transition metals in as-received dpa and GCE were between less than one ppm to tens of ppm (**Tables S1-S2**). This level of metal concentration is many orders of magnitude lower than in metal complex-based ORR catalysts (at a mM level),[40] making ORR activity originating from the traces of the transition metals in dpa and GCE unlikely. Comparative electrochemical experiments were also conducted with sulfuric acids of ACS Plus and Optima® grades, with trace metal contents of less than 0.1 ppm and 1 ppt, respectively. The

ORR polarization curves were identical in both cases (**Figure S1**), confirming no contribution of the trace amounts of the metals to the 2e-ORR.

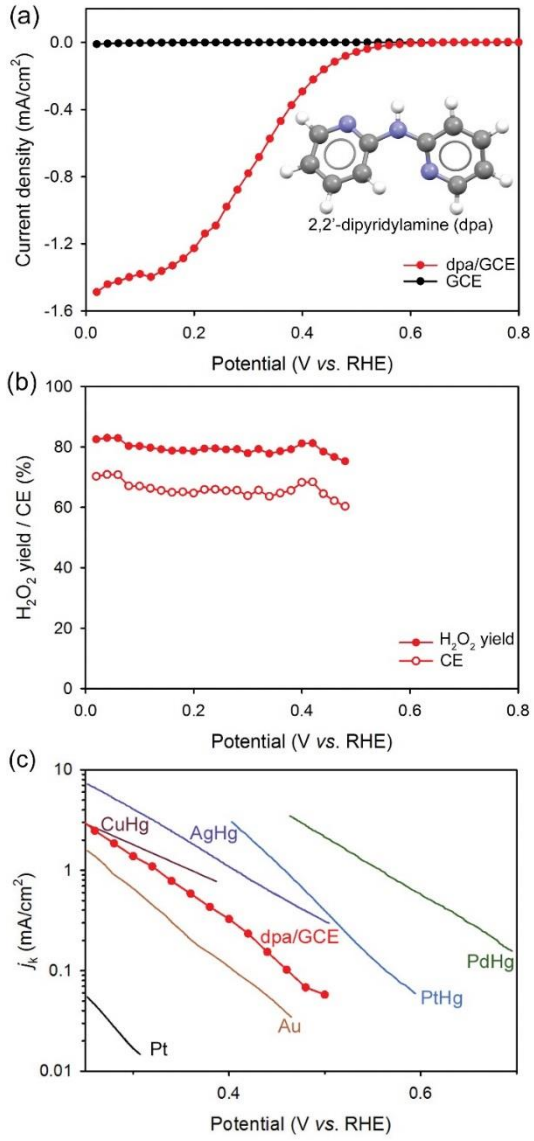

Figure 1. Electrochemical generation of H_2O_2 through two-electron reduction of O_2 at 2,2'-dipyridylamine. (a) RRDE polarization curve of GCE-supported dpa and GCE alone (baseline) in O_2-saturated 0.5 M H_2SO_4; 25 °C, rotation rate 900 rpm, 20 mV potential step, potential hold time 20 s. (b) H_2O_2 yield and current efficiency (CE) determined by RRDE experiment. (c) Kinetic current density for H_2O_2 generation at dpa/GCE and precious metal-based and mercury-based catalysts.

Figure 1c shows a comparison of the 2e-ORR kinetic currents measured with the GCE-supported dpa catalyst and currents measured with precious-metal and mercury-alloy catalysts reported in literature.[17,18] The 2e-ORR activity increases in the order of Pt < Au <

dpa/GCE < Cu-Hg < Ag-Hg < Pt-Hg < Pd-Hg. To account for lower atmospheric pressure at Los Alamos (0.76 atm), the kinetic current at dpa/GCE has been adjusted to one atmosphere pressure, assuming a first-order dependency of 2e-ORR rate on the oxygen pressure (**Figure S2**).[41]

We propose three mechanisms for 2e-ORR at dpa/GCE, which are shown in **Scheme 2**. Mechanism I, catalyzed by dpa molecule, consists of three steps: (1) formation of a dpaHOO intermediate through an oxygen-proton-coupled electron transfer (OPCET) step at dpa; (2) formation of $dpaH_2O_2$ intermediate through a proton-coupled electron transfer (PCET) step; and (3) the dissociation of $dpaH_2O_2$ to release H_2O_2. Mechanism II, catalyzed by singly-protonated dpa ($dpaH^+$) also involves three steps: (1) formation of di-pronated dpa ($dpaH_2^{2+}$) through the protonation of $dpaH^+$; (2) formation of $dpaH_2^+OO$ intermediate through an oxygen-coupled electron transfer (OCET) step; and (3) formation of H_2O_2 and restoration of $dpaH^+$ through a PCET step. Mechanism III, catalyzed by molecular dpa, consists of the following four steps: (1) di-protonation of dpa to $dpaH_2^{2+}$; (2) formation of $dpaH_2^+OO$ intermediate through an OCET step; (3) formation of $dpaH_2O_2$ through an electron transfer (ET) step; and (4) dissociation of $dpaH_2O_2$ into dpa and H_2O_2.

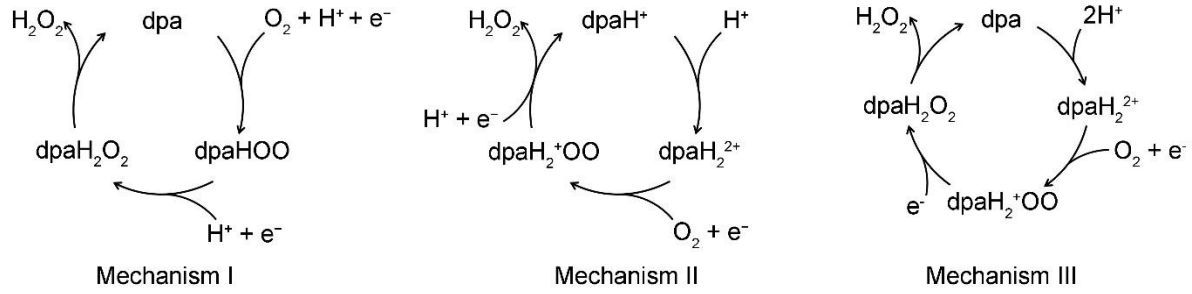

Scheme 2. Proposed 2-e ORR mechanisms at dpa.

We studied the thermodynamics of these three mechanisms using density functional theory (DFT). To simplify the problem, we modeled homogeneous reactions in solution without taking

into account the catalyst-substrate interactions. Three conformers of dpa, namely dpa-A, dpa-B, dpa-C, and intermediates were included in the DFT study. We primarily focused on the intermediates with pyridyl- and amino-N as likely active sites. The calculated Gibbs free energies of reaction intermediates at standard conditions (298.15 K, 1 atm, 1 M solution) are summarized in **Table S3**, and the free energies of reference states are summarized in **Table S4**. The calculated standard reduction potentials ($E°$) for the reduction steps are referenced to the absolute potential of standard hydrogen electrode (E_{SHE} = 4.42 V). The reduction step with the lowest $E°$ along the reaction pathway is referred to in the forthcoming discussion as the thermodynamic potential-determining step.

Figure 2 shows the proposed Mechanism I of H_2O_2 formation at dpa-C, which is the most active among the three possible conformers. The calculated standard reduction potential for dpa-C is 0.48 V *vs*. SHE for the OPCET step and 0.95 V for the PCET step. For dpa-A, the calculated $E°$ for the OPCET step is 0.27 V and 1.12 V for the PCET step. Finally, calculations for dpa-B reveals the $E°$ values of 0.45 V and 0.95 V for OPCET and PCET steps, respectively (**Figures S3-S4**). Of the dpa conformers, dpa-C has been found to be the most active. It should be noted that HOO· is expected to bind to the pyridyl-N and the amine-group hydrogen in dpa-C and dpa-B, and to the pyridyl-N and 2-C hydrogen in dpa-A.

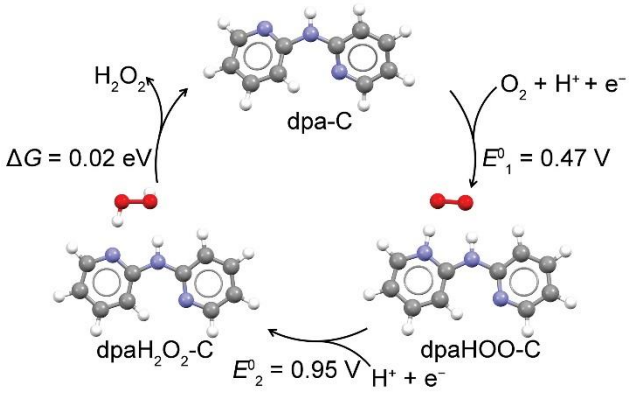

Figure 2. DFT-predicted electrocatalytic H_2O_2-generation cycle with an oxygen-proton-coupled electron transfer step, followed by proton-coupled electron transfer step.

The ORR mechanism on metal surfaces has been the subject of extensive theoretical studies via the computational hydrogen electrode (CHE) approach.[42] Mechanism I at dpa resembles the 2e-ORR mechanism on metal surfaces, proposed in the literature, in which a surface HOO* intermediate is formed (the symbol * denotes a surface species). The HOO* binding energy, ΔG_{HOO*}, was suggested as a thermodynamic descriptor for 2e-ORR activity.[17,18,43] The ΔG_{HOO*} value for an ideal 2e-ORR catalyst with zero thermodynamic limiting potential is 3.52 eV[17,18] at the thermodynamic equilibrium potential for 2e-ORR (U = 0.70 V *vs*. CHE). A ΔG_{HOO*} value lower or higher than 3.52 eV represents an over-binding or under-binding of the HOO* intermediate, respectively, leading to a theoretical thermodynamic overpotential that follows the Sabatier principle (solid black line in **Figure 3b**).[17,18,43] We translated the binding energy of dpa-HOO intermediates from our calculation to ΔG_{HOO*} in the CHE scheme (Supporting Information).[42] **Figure 3a** shows a comparison of the free energy of the HOO* intermediate bound to the conformers of dpa and metallic catalysts at the equilibrium potential for 2e-ORR (U = 0.70 V *vs*. CHE). Of the three dpa conformers, dpa-C shows a HOO* binding energy closest to the ideal catalyst. **Figure 3b** shows the correlation of the 2-e ORR overpotential at a current density of 1.0 mA/cm^2 and ΔG_{HOO*} for dpa-C and metallic H_2O_2 catalysts.

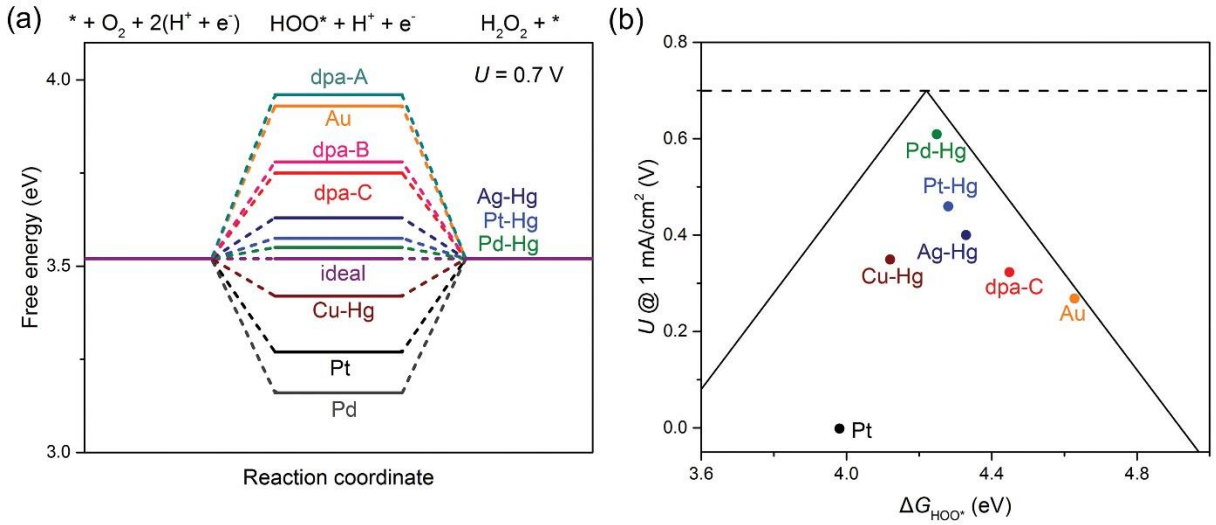

Figure 3. (a) Free-energy diagram showing calculated HOO* binding energy for dpa conformers (dpa-A, dpa-B, and dpa-C) and metallic catalysts. (b) Correlation between overpotential (*U*) required to reach 1 mA/cm^2 current density in H_2O_2 generation and ΔG_{HOO*} for dpa-C conformer and metallic catalysts. Data for metallic catalysts are from literature,[17,18] reported with permission. The solid line in (b) represents a theoretical Sabatier volcano plot for the 2e-ORR overpotential *vs*. ΔG_{HOO*}.[43]

Figure 4 depicts 2-e ORR catalysis according to Mechanisms II and III at dpa-A and dpaH$^+$-A, respectively. The calculated standard reduction potential was 0.71 V for the OCET step at dpa-H_2^{2+}-A, 1.37 V for the PCET step at dpaH_2^+OO-A, and 0.77 V for the ET step at dpaH_2^+OO-A. Of these three steps, the OCET step has the lowest *E*° values, likely becoming the potential-determining step. It should be noticed that the predicted nano-pK_a is a conformation-specific value, which describes the protonation equilibrium between a single protonated conformation and a single deprotonated conformation.[44] It is conceptually different from the micro- or macro-pK_a, as well as experimentally determined pK_a.[44] **Figures S5** and **S6** show the catalytic cycles according to Mechanisms II and III at dpa-B and dpa-C. For dpa-B, the standard reduction potentials are 0.62 V for the OCET step at dpa-H_2^{2+}-B, 0.62 V for the ET step at dpa-H_2^+OO-B, and 1.01 V for the PCET step at dpa-H_2^+OO-B. For dpa-C, the *E*° values are 0.61 V for the OCET step at dpaH_2^{2+}-C, 0.61 V for the ET step at dpa-H_2^+OO-C, and 1.05 V for the PCET step at dpa-H_2^+OO-C. The results suggest that dpa-A has higher activity for 2e-ORR proceeding

according to Mechanisms II and III than dpa-B and dpa-C. Also, the thermodynamic potential-determining steps in Mechanisms II and III have $E°$ higher than those in Mechanism I, implying that Mechanisms II and III are favored over Mechanism I. As suggested by the results of DFT calculations, various dpa conformers and their conjugated acids have different catalytic activities. It is thus plausible that the apparent activity of the dpa on GDE depends on the conformational ensembles of dpa at equilibrium under given electrochemical conditions.

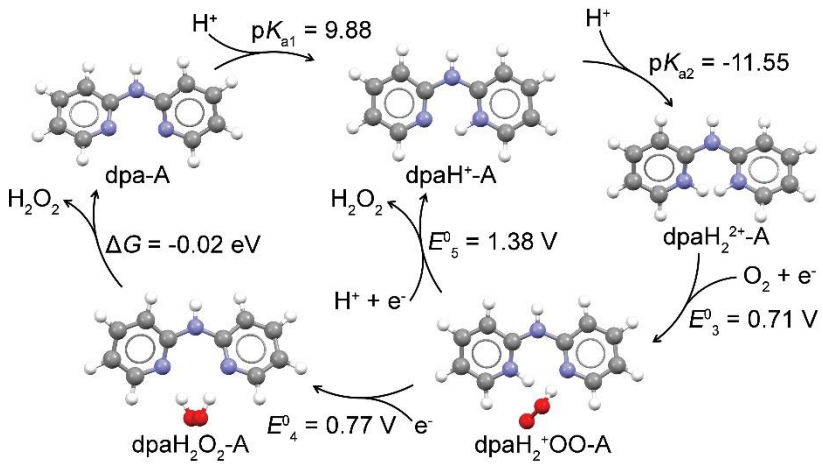

Figure 4. DFT-predicted catalytic cycle for 2e-ORR at dpa-A and its conjugated acids. Cycle consists of an oxygen-coupled electron transfer step and a proton-coupled electron transfer step (Mechanism II) or a single-electron transfer step (Mechanism III).

Figure S7 shows a durability test of the dpa/GCE catalyst during H_2O_2 generation at a constant potential of 0 V *vs*. RHE in 0.5 M H_2SO_4. A decrease in the reduction current was observed during the first five hours and continued until reaching a steady current after approximately 10 hours. A steady-state polarization recorded after 20 hours of the durability testing shows a decrease in 2e-ORR activity. The H_2O_2 yield increased from *ca*. 80% to *ca*. 98% after the durability test (**Figure S8**). The detailed mechanism of the change in catalytic activity and selectivity over time at 0 V vs. RHE is still unclear and will be addressed in our future research. It is possible that the

equilibrium conformational ensembles of dpa change during the durability test, leading to the observed change in activity.

Conclusions

Summarizing, we demonstrate in this work, a new type of 2e-ORR electrocatalyst, which is based on a small organic molecule, dpa. As acid compatible, heterogeneous catalyst composed of abundant C, N, H elements, dpa is capable of catalyzing the electrochemical generation of hydrogen peroxide from dioxygen at low overpotentials (high rates) with high selectivity in aqueous acidic electrolyte. These properties make dpa appealing for the application of hydrogen peroxide production in electrochemical devices for clean energy conversion and water treatment. The DFT study reveals possible 2e-ORR mechanisms at dpa, in which the pyridyl- and amino-N play as the anchoring sites for reaction intermediates. The results of DFT calculations also suggest strong dependence of the dpa activity on the molecule conformation, which determines its thermodynamic limiting potentials. This research opens up the possibility for molecular design of organic compounds for electrochemical production of H_2O_2 and helps understand the electrochemical properties of C-N based materials.

Experimental

Materials. 2,2′-dipyridylamine (dpa, 98%, Sigma-Aldrich), chloroform (99%, Sigma-Aldrich), isopropanol (IPA, > 99.5%, Certified ACS Plus Grade, Fisher Chemical), sulfuric acid ((H_2SO_4, 97.2 wt%, Certified ACS Plus Grade lot# 153943, and 95 wt%, Optima® lot# 3217051, Fisher

Chemical)), hydrogen gas (H_2, 99.999%, Airgas Inc.), nitrogen gas (N_2, 99.999%, Airgas Inc.), and oxygen gas (O_2, 99.999%, Airgas Inc.) were used as received.

Electrode preparation. ORR activity of dpa adsorbed on glassy carbon electrode (GCE) was studied using an E6R1 ChangeDisk® rotating ring disk electrode (RRDE, Pine Research Instrumentation). The working electrode was a 5.0 mm in diameter interchangeable glassy carbon disk (Pine Research Instrumentation). Before each experiment, the glassy carbon disk insert was first sanded with a fresh of 600-grit CarbiMet® paper and then polished with 0.3 μm and 0.05 μm alumina suspensions on nylon and MicroCloth (Buehler) polishing clothes, respectively, before being sonicated in the isopropanol bath three times. The thus-prepared glassy carbon disk was inserted into the RRDE tip and immersed into 1.0 M solution of dpa in chloroform to allow dpa to adsorb for three hours. At the end of adsorption, the electrode was removed from the dpa solution, immediately dried in air and rinsed with 0.5 M H_2SO_4 solution to remove the excess dpa.

Electrochemical measurements. The electrochemical measurements were performed in an electrochemical cell filled with 0.5 M H_2SO_4 supporting electrolyte, using a CHI 760D potentiostat (CH Instruments). A graphite rod served for the counter electrode. A hydrogen reference electrode (HydroFlex®, Gaskatel GmbH) was used and calibrated versus a reversible hydrogen electrode (RHE). The working electrode was cycled between -0.5 and 0.3 V *vs*. RHE at a scan rate of 20 mV/s, first at 80 °C and then at 25 °C in N_2-saturated 0.5 M H_2SO_4. The ORR performance was measured by staircase voltammetry from 0.8 to 0 V *vs*. RHE at steps of 20 mV, 20 s per step, at a rotation rate of 900 rpm in O_2-saturated 0.5 M H_2SO_4. Ring current was measured at a ring potential of 1.3 V *vs*. RHE. The collection efficiency of the Pt ring, *N*, was determined to be 23% using the reversible redox $[Fe(CN)_6]^{4-/3-}$ couple (0.36 V *vs*. SHE). The yield of H_2O_2, Y_{H2O2}, and the current efficiency, *CE*, were calculated using the following equations:

$$Y_{H2O2} = 200\%(I_r/N)/(I_d+I_r/N) \quad \text{(Eq. 1)}$$

$$CE = 2Y_{H2O2}/(400\% - 2Y_{H2O2}) \quad \text{(Eq. 2)}$$

where I_r is the ring current and I_d is the disk current.

The kinetic current density j_k was calculated using the equation:

$$1/j = 1/j_d + 1/j_k \quad \text{(Eq. 3)}$$

where j is the total current density and j_d is the measured mass transport-limited current density. The kinetic current density presented in Figure 1c was divided by a factor of 0.76 for a fair comparison with the reference data measured at 1 atm, assuming a first-order dependency of 2e-ORR rate on the concentration of oxygen concentration (see above).[41]

The theoretical limiting current density at Los Alamos elevation was calculated using the equation:

$$j_d = (0.620)nFD^{2/3}\nu^{-1/6}C_O\,\omega^{1/2} \quad \text{(Eq. 4)}$$

where n is the number of electrons transferred in half-reaction (2 for 2e-ORR, 4 for 4e-ORR), F is the Faraday constant (96485 C/mol), D is the diffusion coefficient of oxygen ($1.9\ 10^{-5}$ cm^2/s), ν is the kinematic viscosity of water ($0.890\ 10^{-2}$ cm^2/s),[45] C_O is the concentration of O_2 in 0.5 M H_2SO_4 ($1.026\ 10^{-6}$ mol/cm^3 at 1 atm,[46] 0.76 atm at the Los Alamos altitude), ω is the angular rotation rate of the electrode (900 rpm; 94.248 rad/s). The theoretical j_d is *ca*.1.42 mA/cm^2 for 100% 2e-ORR.

Theoretical Calculations

Computational details. DFT calculations were carried out using Gaussian 09 package at B3LYP/6-31++G(d,p) level of theory, with a geometric optimization of the structures followed by

a single-point energy and frequency calculation. The electrostatic solute-solvent interactions were treated with the Polarizable Continuum Model (PCM), using the integral equation formalism variant (IEFPCM) and water as the solvent. An extension of the dpa catalyst name was used to differentiate the conformational structures, *e.g.*, dpa-A, dpa-B, and dpa-C. The calculated Gibbs free energy values at standard conditions (298.15 K, 1.0 atm, 1 M concentration) are summarized in Table S2.

The standard reduction potential $E°$ was calculated according to the equation:

$$E° = -\Delta G/nF - E_{SHE} \quad \text{(Eq. 5)}$$

where ΔG is the free molar energy of reaction, n is the number of electrons in the half-reaction, F is the Faraday constant, E_{SHE} is the absolute potential of the aqueous standard hydrogen electrode (SHE). The value of E_{SHE} is 4.42 V, based on the experimental values of the proton solvation energy, $\Delta G^*_S(H^+)$, of -1091 kJ/mol, and the proton formation energy, $\Delta_f G^0$ (H^+), of 1517 kJ/mol.

For a single-electron reduction reaction: Ox + e^- → Red, Ox: oxidized species, Red: reduced species, the free molar energy of reaction, ΔG, is calculated according to the equation:

$$\Delta G = G(\text{Red}) - (G(\text{Ox}) + G(e^-)) \quad \text{(Eq. 6)}$$

where $G(e^-)$ is the free energy of the free electron gas, with the values of -0.001383 Hartree (-3.632 kJ/mol) by convention.

The free energy of the solvated proton, $G(H^+)$, was calculated to be -0.426352 Hartree according to the equation:

$$G(H^+) = G(H_2)/2 + 4.42\ \text{eV} - G(e^-) \quad \text{(Eq. 7)}$$

where $G(H_2)$ is the Gibbs free energy of hydrogen gas from DFT calculation.

At 298.15 K 1 atm, liquid water is in equilibrium with 0.03128 atm H_2O vapor, therefore the free energy of water is calculated according to the equation:

$$G(H_2O \text{ liquid, 1 atm}) = G(H_2O \text{ gas, 0.03128 atm}) \quad \text{(Eq. 8)}$$

where $G(H_2O$ gas, 0.03128 atm) is the Gibbs free energy of H_2O gas at 0.03128 atm from DFT calculation.

The free energy of O_2, $G(O_2)$, was calculated according to the equation:

$$G(O_2) = 2\times G(H_2O, \text{liquid, 1.0 atm}) - 2\times G(H_2) + 4e\times 1.23 \text{ V} \quad \text{(Eq. 9)}$$

where 1.23 V is the standard electrode potential for the reaction: $2O_2 + 4H^+ + 4e^- \rightarrow 2H_2O_2$

The free energy of H_2O_2, $G(H_2O_2)$, was calculated according to the equation:

$$G(H_2O_2) = G(O_2) + 2\times[G(H^+) + G(e^-) - 4.42 \text{ eV}] - 2e\times 0.70 \text{ V} \quad \text{(Eq. 10)}$$

$$G(H_2O_2) = G(O_2) + G(H_2) - 2e\times 0.70\text{V} \quad \text{(Eq. 11)}$$

where 0.70 V is the standard reduction potential $E°$ for reaction:

$$O_2 + 2H^+ + 2e^- \rightarrow H_2O_2$$

The nano-pK_a values of the conjugated acids in specific conformations were calculated using the equation:

$$pK_a = \Delta G_{AH+/A}/(2.303RT) \quad \text{(Eq.12)}$$

where $\Delta G_{AH+/A}$ is the acid dissociation energy of the conjugated acid in specific conformations, R is the ideal gas constant, T is the temperature (298.15 K).

ASSOCIATED CONTENT

Supporting Information.

The following files are available free of charge: Supporting Information (PDF)

AUTHOR INFORMATION

Corresponding Author

*zelenay@lanl.gov

Funding Sources

Los Alamos National Laboratory, Laboratory Directed Research and Development program, Exploratory Research (LDRD-ER)

ACKNOWLEDGMENTS

The authors would like to thank Edward Holby for helpful discussions and Hoon Chung, Geraldine Purdy, and Mahlon Wilson for technical help with this research. Financial support of this research by DOE-EERE through Fuel Cell Technologies Office and by Los Alamos National Laboratory through Laboratory Directed Research and Development (LDRD) program is gratefully acknowledged. L. L. is grateful for the support from China Scholarship Council (SCS).

ABBREVIATIONS

GCE, glassy carbon electrode; dpa, 2,2'-dipyridylamine; dpa/GCE, dpa on glassy carbon disk electrode; 2e-ORR, two-electron oxygen reduction reaction; RRDE, rotating ring-disk electrode;

RDE, rotating-disk electrode; RHE, reversible hydrogen electrode; SHE, standard hydrogen electrode; CE, current efficiency; PCET, proton-coupled electron transfer; OPCET, oxygen-proton-coupled electron transfer; OCET, oxygen-coupled electron transfer; ET, electron transfer; CHE, computational hydrogen electrode.

REFERENCES

(1) Campos-Martin, J. M.; Blanco-Brieva, G.; Fierro, J. L. G., Hydrogen Peroxide Synthesis: An Outlook beyond the Anthraquinone Process. *Angew. Chem. Int. Ed.* **2006,** *45*, 6962-6984.

(2) Centi, G.; Perathoner, S.; Abate, S., Direct Synthesis of Hydrogen Peroxide: Recent Advances. In *Modern Heterogeneous Oxidation Catalysis*, Wiley-VCH Verlag GmbH & Co. KGaA: 2009; pp 253-287.

(3) Yamanaka, I.; Murayama, T., Neutral H_2O_2 Synthesis by Electrolysis of Water and O_2. *Angew. Chem. Int. Ed.* **2008,** *47*, 1900-1902.

(4) Yamanaka, I.; Onizawa, T.; Takenaka, S.; Otsuka, K., Direct and Continuous Production of Hydrogen Peroxide with 93 % Selectivity Using a Fuel-Cell System. *Angew. Chem. Int. Ed.* **2003,** *42*, 3653-3655.

(5) Ichiro, Y.; Toshihide, H.; Kiyoshi, O., Direct Synthesis of Hydrogen Peroxide (>1 wt%) over the Cathode Prepared from Active Carbon and Vapor-Grown-Carbon-Fiber by a New H_2–O_2 Fuel Cell System. *Chem. Lett.* **2002,** *31*, 852-853.

(6) Yamanaka, I.; Onisawa, T.; Hashimoto, T.; Murayama, T., A Fuel-Cell Reactor for the Direct Synthesis of Hydrogen Peroxide Alkaline Solutions from H_2 and O_2. *ChemSusChem* **2011,** *4*, 494-501.

(7) Choi, J.; Hwang, S. H.; Jang, J.; Yoon, J., High Yield Hydrogen Peroxide Production in a Solid Polymer Electrolyte Electrolyzer with a Carbon Fiber Coated Mesh Substrate. *Electrochem. Commun.* **2013,** *30*, 95-98.

(8) Abdullah, G. H.; Xing, Y., Hydrogen Peroxide Generation in Divided-Cell Trickle Bed Electrochemical Reactor. *Ind. Eng. Chem. Res.* **2017,** *56*, 11058-11064.

(9) Lu, Z.; Chen, G.; Siahrostami, S.; Chen, Z.; Liu, K.; Xie, J.; Liao, L.; Wu, T.; Lin, D.; Liu, Y.; Jaramillo, T. F.; Nørskov, J. K.; Cui, Y., High-Efficiency Oxygen Reduction to Hydrogen Peroxide Catalysed by Oxidized Carbon Materials. *Nat. Catal.* **2018,** *1*, 156-162.

(10) Chen, S.; Chen, Z.; Siahrostami, S.; Kim, T. R.; Nordlund, D.; Sokaras, D.; Nowak, S.; To, J. W. F.; Higgins, D.; Sinclair, R.; Nørskov, J. K.; Jaramillo, T. F.; Bao, Z., Defective Carbon-Based Materials for the Electrochemical Synthesis of Hydrogen Peroxide. *ACS Sustain. Chem. Eng.* **2017,** *6*, 311-317.

(11) Kim, H. W.; Ross, M. B.; Kornienko, N.; Zhang, L.; Guo, J.; Yang, P.; McCloskey, B. D., Efficient Hydrogen Peroxide Generation using Reduced Graphene Oxide-Based Oxygen Reduction Electrocatalysts. *Nat. Catal.* **2018,** *1*, 282-290.

(12) Fellinger, T.-P.; Hasché, F.; Strasser, P.; Antonietti, M., Mesoporous Nitrogen-Doped Carbon for the Electrocatalytic Synthesis of Hydrogen Peroxide. *J. Am. Chem. Soc.* **2012,** *134*, 4072-4075.

(13) Hasché, F.; Oezaslan, M.; Strasser, P.; Fellinger, T.-P., Electrocatalytic Hydrogen Peroxide Formation on Mesoporous Non-Metal Nitrogen-Doped Carbon Catalyst. *J. Energy Chem.* **2016,** *25*, 251-257.

(14) Park, J.; Nabae, Y.; Hayakawa, T.; Kakimoto, M.-a., Highly Selective Two-Electron Oxygen Reduction Catalyzed by Mesoporous Nitrogen-Doped Carbon. *ACS Catal.* **2014,** *4*, 3749-3754.

(15) Choi, C. H.; Kwon, H. C.; Yook, S.; Shin, H.; Kim, H.; Choi, M., Hydrogen Peroxide Synthesis via Enhanced Two-Electron Oxygen Reduction Pathway on Carbon-Coated Pt Surface. *J. Phys. Chem. C* **2014,** *118*, 30063-30070.

(16) Choi, C. H.; Kim, M.; Kwon, H. C.; Cho, S. J.; Yun, S.; Kim, H.-T.; Mayrhofer, K. J. J.; Kim, H.; Choi, M., Tuning Selectivity of Electrochemical Reactions by Atomically Dispersed Platinum Catalyst. *Nat. Commun.* **2016,** *7*, 10922.

(17) Siahrostami, S.; Verdaguer-Casadevall, A.; Karamad, M.; Deiana, D.; Malacrida, P.; Wickman, B.; Escudero-Escribano, M.; Paoli, E. A.; Frydendal, R.; Hansen, T. W.; Chorkendorff, I.; Stephens, I. E. L.; Rossmeisl, J., Enabling Direct H_2O_2 Production Through Rational Electrocatalyst Design. *Nat. Mater.* **2013,** *12*, 1137-1143.

(18) Verdaguer-Casadevall, A.; Deiana, D.; Karamad, M.; Siahrostami, S.; Malacrida, P.; Hansen, T. W.; Rossmeisl, J.; Chorkendorff, I.; Stephens, I. E. L., Trends in the Electrochemical Synthesis of H_2O_2: Enhancing Activity and Selectivity by Electrocatalytic Site Engineering. *Nano Lett.* **2014,** *14*, 1603-1608.

(19) Tammeveski, K.; Kontturi, K.; Nichols, R. J.; Potter, R. J.; Schiffrin, D. J., Surface Redox Catalysis for O_2 Reduction on Quinone-Modified Glassy Carbon Electrodes. *J. Electroanal. Chem.* **2001,** *515*, 101-112.

(20) Kullapere, M.; Seinberg, J.-M.; Mäeorg, U.; Maia, G.; Schiffrin, D. J.; Tammeveski, K., Electroreduction of Oxygen on Glassy Carbon Electrodes Modified with in situ Generated Anthraquinone Diazonium Cations. *Electrochim. Acta* **2009,** *54*, 1961-1969.

(21) Sarapuu, A.; Vaik, K.; Schiffrin, D. J.; Tammeveski, K., Electrochemical Reduction of Oxygen on Anthraquinone-Modified Glassy Carbon Electrodes in Alkaline Solution. *J. Electroanal. Chem.* **2003,** *541*, 23-29.

(22) Jürmann, G.; Schiffrin, D. J.; Tammeveski, K., The pH-Dependence of Oxygen Reduction on Quinone-Modified Glassy Carbon Electrodes. *Electrochim. Acta* **2007,** *53*, 390-399.

(23) Bird, C. L.; Kuhn, A. T., Electrochemistry of the Viologens. *Chem. Soc. Rev.* **1981,** *10*, 49-82.

(24) Martigny, P.; Anson, F. C., Catalysis of the Reduction of Dioxygen by Poly(xylylviologen) Coatings on Graphite Electrodes. *J. Electroanal. Chem.* **1982,** *139*, 383-393.

(25) Andrieux, C. P.; Hapiot, P.; Sa Véant, J. M., Electron Transfer Coupling of Diffusional Pathways. Homogeneous Redox Catalysis of Dioxygen Reduction by the Methylviologen Cation Radical in Acidic Dimethylsulfoxide. *J. Electroanal. Chem.* **1985,** *189*, 121-133.

(26) Nolan, J. E.; Plambeck, J. A., The EC-Catalytic Mechanism at the Rotating Disk Electrode: Part II. Comparison of Approximate Theories for the Second-Order Case and Application to the Reaction of Bipyridinium Cation Radicals with Dioxygen in Non-Aqueous Solutions. *J. Electroanal. Chem.* **1990,** *294*, 1-20.

(27) Oh, M.-K.; Okajima, T.; Kitamura, F.; Lee, C.-W.; Tokuda, K.; Ohsaka, T., Electrocatalytic Reduction of Dioxygen in the Presence of *N*,*N*'-Dipentyl Viologen. *Chem. Lett.* **1997,** *26*, 67-68.

(28) Oyama, N.; Oki, N.; Ohno, H.; Ohnuki, Y.; Matsuda, H.; Tsuchida, E., Electrocatalytic Reduction of Oxygen by Poly(viologen)-Poly (sulfonate) Complex Coated on Graphite Electrodes. *J. Phys. Chem.* **1983,** *87*, 3642-3647.

(29) Wang, R.; Okajima, T.; Kitamura, F.; Kawauchi, S.; Matsumoto, N.; Thiemann, T.; Mataka, S.; Ohsaka, T., Catalytic Reduction of O_2 by Pyrazine Derivatives. *J. Phys. Chem. A* **2004,** *108*, 1891-1899.

(30) Ohsaka, T.; Watanabe, T.; Kitamura, F.; Oyama, N.; Tokuda, K., Electrocatalysis of Poly(2,3-diaminonaphthalene)-Filmed Electrodes for Reduction of Oxygen. *J. Chem. Soc., Chem. Commun.* **1991,** (7), 487-489.

(31) Ohsaka, T.; Watanabe, T.; Kitamura, F.; Oyama, N.; Tokuda, K., Electrocatalysis of O_2 Reduction at Poly(o-phenylenediamine)- and Poly(o-aminophenol)-Coated Glassy Carbon Electrodes. *J. Chem. Soc., Chem. Commun.* **1991,** (16), 1072-1073.

(32) Briega-Martos, V.; Ferre-Vilaplana, A.; de la Peña, A.; Segura, J. L.; Zamora, F.; Feliu, J. M.; Herrero, E., An Aza-Fused π-Conjugated Microporous Framework Catalyzes the Production of Hydrogen Peroxide. *ACS Catal.* **2017,** *7*, 1015-1024.

(33) Trojanek, A.; Langmaier, J.; Sebera, J.; Zalis, S.; Barbe, J.-M.; Girault, H. H.; Samec, Z., Fine Tuning of the Catalytic Effect of a Metal-Free Porphyrin on the Homogeneous Oxygen Reduction. *Chem. Commun.* **2011,** *47*, 5446-5448.

(34) Hatay, I.; Su, B.; Méndez, M. A.; Corminboeuf, C.; Khoury, T.; Gros, C. P.; Bourdillon, M.; Meyer, M.; Barbe, J.-M.; Ersoz, M.; Záliš, S.; Samec, Z.; Girault, H. H., Oxygen Reduction

Catalyzed by a Fluorinated Tetraphenylporphyrin Free Base at Liquid/Liquid Interfaces. *J. Am. Chem. Soc.* **2010,** *132*, 13733-13741.

(35) Mase, K.; Ohkubo, K.; Xue, Z.; Yamada, H.; Fukuzumi, S., Catalytic Two-Electron Reduction of Dioxygen Catalysed by Metal-Free [14]triphyrin(2.1.1). *Chem. Sci.* **2015,** *6*, 6496-6504.

(36) Wu, S.; Su, B., Metal-Free-Porphyrin-Catalyzed Oxygen Reduction at Liquid–Liquid Interfaces. *Chem. Eur. J.* **2012,** *18*, 3169-3173.

(37) Trojánek, A.; Langmaier, J.; Samec, Z., Thermodynamic Driving Force Effects in the Oxygen Reduction Catalyzed by a Metal-Free Porphyrin. *Electrochim. Acta* **2012,** *82*, 457-462.

(38) Trojánek, A.; Langmaier, J.; Záliš, S.; Samec, Z., Mechanistic Model of the Oxygen Reduction Catalyzed by a Metal-Free Porphyrin in One- and Two-Phase Liquid Systems. *Electrochim. Acta* **2013,** *110*, 816-821.

(39) Liu, X.; Wu, S.; Su, B., Oxygen Reduction with Tetrathiafulvalene at Liquid/Liquid Interfaces Catalyzed by 5,10,15,20-Tetraphenylporphyrin. *J. Electroanal. Chem.* **2013,** *709*, 26-30.

(40) Pegis, M. L.; Wise, C. F.; Martin, D. J.; Mayer, J. M., Oxygen Reduction by Homogeneous Molecular Catalysts and Electrocatalysts. *Chem. Rev.* **2018,** *118*, 2340-2391.

(41) Wang, J. X.; Uribe, F. A.; Springer, T. E.; Zhang, J.; Adzic, R. R., Intrinsic Kinetic Equation for Oxygen Reduction Reaction in Acidic Media: the Double Tafel Slope and Fuel Cell Applications. *Faraday Discuss.* **2009,** *140*, 347-362.

(42) Nørskov, J. K.; Rossmeisl, J.; Logadottir, A.; Lindqvist, L.; Kitchin, J. R.; Bligaard, T.; Jónsson, H., Origin of the Overpotential for Oxygen Reduction at a Fuel-Cell Cathode. *J. Phys. Chem. B* **2004,** *108*, 17886-17892.

(43) Viswanathan, V.; Hansen, H. A.; Rossmeisl, J.; Nørskov, J. K., Unifying the 2e– and 4e– Reduction of Oxygen on Metal Surfaces. *J. Phys. Chem. Lett.* **2012,** *3*, 2948-2951.

(44) Bochevarov, A. D.; Watson, M. A.; Greenwood, J. R.; Philipp, D. M., Multiconformation, Density Functional Theory-Based pK_a Prediction in Application to Large, Flexible Organic Molecules with Diverse Functional Groups. *J. Chem. Theory Comput.* **2016,** *12*, 6001-6019.

(45) *CRC Handbook of Chemistry and Physics*. 99th Edition (Internet Version 2018) ed.; CRC Press/Taylor & Francis: Boca Raton, FL.

(46) Gubbins, K. E.; Walker, R. D., The Solubility and Diffusivity of Oxygen in Electrolytic Solutions. *J. Electrochem. Soc.* **1965,** *112*, 469-471.